European Journal of Control (2011)3:261–272

DOI:10.3166/EJC.17.261–272

European Journal of Control

Model-Based Feedforward Control of Large Deformable Mirrors

Thomas Ruppel[1,*], Wolfgang Osten[2], Oliver Sawodny[1]

[1] Institut für Systemdynamik, Pfaffenwaldring 9, Universität Stuttgart, 70569 Stuttgart, Germany;
[2] Institut für Technische Optik, Pfaffenwaldring 9, Universität Stuttgart, 70569 Stuttgart, Germany

In this paper, a model-based feedforward control concept for fast set-point changes of large deformable mirrors is proposed. It takes into account local position control loops of excited actuators and mode-dependent stiffness variations of the mirror shell. Based on partial differential equations for the temporal and spatial behavior of the deformable mirror, a modal approximation of the mirror dynamics is performed. It is shown that a second order approximation of the eigenmode dynamics is appropriate for low-order modes even when additional system components as delays, digital-to-analog converters, current drivers, actuator-magnet efficiencies, capacitive sensors, and analog-to-digital converters are included. In particular, appropriate transfer functions with identified coefficients of the proposed modal models are presented for a 45-actuator prototype of the Large Binocular Telescope adaptive secondary mirror (P45). Additionally, experimental results with model-based feedforward control are presented. The identified dynamic model of the P45 is finally used to derive flatness based feedforward commands for chopping.

Keywords: Deformable mirror, feedforward control, modal control, flatness based control

1. Introduction

In the last 10 years, deformable secondary mirrors have proven to be an essential technology for ground based astronomical adaptive optics. Starting with a 642 mm wide and 2 mm thick continuous face-sheet deformable mirror for the Multi Mirror Telescope (MMT), new deformable mirrors with diameters around 1000 mm are built for e.g. the Large Binocular Telescope (LBT) and the Very Large Telescope (VLT) [1, 5, 6, 18]. With over thousand voice coil actuators, this generation of continuous face-sheet deformable mirrors requires fast and precise position control. Thereby, the main idea for robust control of the mirror deflection is the use of distributed voice coil actuators in combination with local position sensing by capacitive sensors. The use of voice coil actuators allows for large stroke and exact positioning of the mirror while it is floating in a magnetic field. By changing the spatial properties of the magnetic field, the mirror shell can be deformed into a desired position to compensate for optical aberrations. Thereby, a low-contact bearing combined with little intrinsic damping of the mirror shell draws the need for adequate damping in closed loop operation. For the MMT deformable mirror, this problem is tackled by a 40 μm air-gap between the mirror shell and a reference plate behind the shell. The induced viscous damping is sufficient to operate the mirror within the designed specifications [6]. Although, future deformable mirrors will operate within a larger air-gap to provide more stroke. As a side effect, the larger air-gap reduces the natural viscous damping and electronic damping is needed to achieve the same control bandwidth [20].

Currently, the standard control approach for deformable mirrors of the LBT and VLT type is local PD-control for each actuator in combination with feedforward force

*Correspondence to: T. Ruppel, E-mail: thomas.ruppel@isys.uni-stuttgart.de

Received 04 December 2009; Accepted 3 August 2010
Recommended by C. Kulcsár, H.-F. Raynaud, J.-M. Conan, D.W. Clarke

compensation [4]. Thereby, each actuator is driven by a dedicated local position controller running at 40–70 kHz. The shape command for the mirror unit is generated by a higher level wavefront control loop running at about 1 kHz. For small set-point changes of the mirror shell, this control concept is well-suited and has proven to be applicable in practice [7]. Although, for high speed deformations over large phase changes (e.g. chopping), disadvantages of local PD-control must be considered. First of all, there is a shape-dependent stiffness and damping variation of the mirror shell. In particular, each deformation of the shell requires a specific amount of external force to be kept in shape [6]. If local control instead of global control is used for position control of the shell, then robust and subsequently conservative controller design is necessary for all local control loops. Secondly, interaction of neighboring actuators has to be studied carefully. The control loop gains have to be chosen such that only little influence on neighboring actuators is achieved. Otherwise, the local control concept can lead to instability of the shell.

To further investigate alternative control concepts, there have been studies on MIMO optimal control of deformable mirrors [17, 28, 2]. Certainly, the closed loop performance of a global optimal control concept is superior to local PD-control. But still, the computational load of a global MIMO controller may not be suitable for large deformable mirrors with more than thousand actuators. Only in [17], the circular symmetry of the mirror shell is used to reduce the controllers complexity. Thereby, it is shown that symmetry can effectively reduce computational loads without loosing control performance. Although, even when symmetry is fully exploited, the computational effort for a global 1000 actuator control concept of future deformable mirrors is considerably high.

In this paper, a different approach for control of large deformable mirrors is proposed. Clearly, the most difficult control task for large deformable mirrors is not the stabilization of the shell in a static shape, but changing the mirrors deflection in a predefined time while maintaining system stability. Instead of designing a feedback controller for this task, a model-based feedforward control concept is proposed. In the past, the concept of model-based feedforward control has successfully been applied to various classes of dynamical systems [9]. This technique is widely used in control practice as an extension of a feedback control loop to separately design tracking performance by the feedforward part and closed-loop stability and robustness by the feedback part. By using model-based feedforward control for set-point changes of a mirror shell, the local control loops are only needed to stabilize the shell in steady state and along precomputed trajectories. Thereby, the local control loops can be designed to achieve high disturbance rejection. The computational load for feedforward control is comparably low because the feedforward signals may not be computed in the local control loop frequency of the position control loops (40–70 kHz), but only when a new set-point is commanded (about 1 kHz).

In this work, the proposed feedforward control concept is based on a modal approximation of the mirror dynamics. Each deflection of the mirror shell is transformed into modal coordinates composed by the dynamic eigenmodes. For a set-point change of the mirror's deflection, each mode is changed independently and controlled by feedforward forces in a time optimal manner. The internal control loops account for model errors and external disturbances along the computed trajectories and can be implemented as PD-control, for example. If a suitable dynamic model of the mirror shell can be derived, then the dominant control forces are given by the feedforward control signal. In earlier work, this concept has proven to be applicable for a set-point change in piston [22]. The expansion of this idea to intrinsic eigenmodes of the mirror shell and its application to chopping is described in this paper. Accounting for future large deformable mirrors, a more general trajectory generation concept for higher order modes with inherent zero-dynamics is proposed, also. Thereby, the formalism of flatness based feedforward control [10] is applied to the modal dynamics of the mirror.

The structure of the paper is as follows: In Section 2, an analytic model of a continuous face-sheet deformable mirror together with suitable boundary conditions is derived. The analytic solution of the resulting partial differential equation and its usability for feedforward control design is discussed. In Section 3, modal identification results of a 45 actuator prototype deformable mirror (P45) of the LBT type are presented. Hereby, it is shown that for low order modes the typical second order approximation of closed loop modal transfer functions is favorable even with inclusion of additional system components as delays, digital-to-analog converters, current drivers, actuator-magnet efficiencies, capacitive sensors, and analog-to-digital converters. In Section 4, the generation of model-based feedforward trajectories is described. Different types of motion primitives are discussed and an example for practical implementation is given. In Section 5, experimental results of a set-point change with model-based feedforward control are given. Additionally, the challenging task of mirror chopping is addressed and simulation results of model-based feedforward trajectories for chopping are presented. Thereby, the simulations are based on identified eigenmodes of the P45. Conclusions and an outlook to future work are given in Section 6.

2. Mirror Modeling

A detailed mechanical description of the considered deformable mirrors can be found in [21]. Here, of

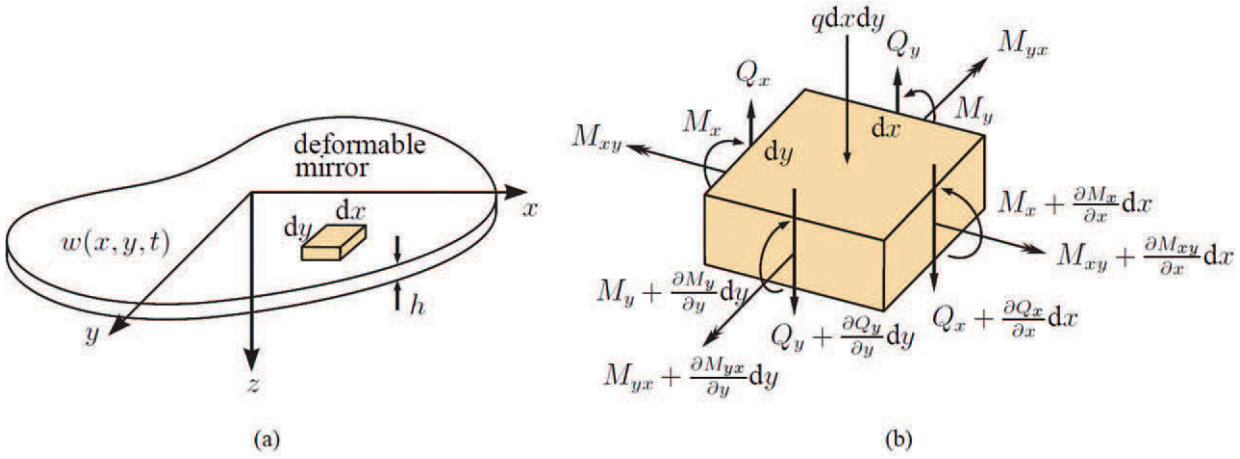

Fig. 1. Governing forces and moments (b) for a differential plate element of thickness h (a).

particular interest is the deformable mirror surface with free edges at the inner and outer radius r_1 and r_2, respectively. Although the face-sheet is only 1.6 mm thick, it still has a considerable out-of-plane stiffness and is modeled as a thin Kirchhoff plate. As discussed in [27], a large radius of curvature and a large diameter of the deformable mirror spherical face-sheet (approx. 2 m) in comparison to the considered deflections (approx. 100 µm) allows to approximate the spherical shell by a Kirchhoff plate. Similar assumptions are drawn in [12] for a comparable system. Therefore, it is assumed that the native curvature of the shell can be neglected due to only small deflections perpendicular to the surface.

The governing forces for a differential element of the plate are shown in Fig. 1. The plate of thickness h and of infinite extent is expected to have its undeflected surface in the x, y-plane. The differential element $h\mathrm{d}x\mathrm{d}y$ is effected by various shear forces, bending and twisting moments, and external loads as illustrated in Fig. 1. The bending moments per unit length M_x, M_y arise from distributions of normal stresses σ_x, σ_y, while the twisting moments per unit length M_{xy}, M_{yx} (shown as double-arrow vectors) arise from shearing stresses τ_{xy}, τ_{yx}. The shear forces per unit length Q_x, Q_y arise from shearing stresses τ_{xz}, τ_{yz} [11].

Of particular interest are the resulting three equations of motion

$$-Q_x\mathrm{d}y + \left(Q_x + \frac{\partial Q_x}{\partial x}\mathrm{d}x\right)\mathrm{d}y - Q_y\mathrm{d}x + \left(Q_y + \frac{\partial Q_y}{\partial y}\mathrm{d}y\right)\mathrm{d}x + q\mathrm{d}x\mathrm{d}y = \rho h\mathrm{d}x\mathrm{d}y\frac{\partial^2 w}{\partial t^2}, \quad (1a)$$

$$\left(M_y + \frac{\partial M_y}{\partial y}\mathrm{d}x\right)\mathrm{d}x - M_y\mathrm{d}x + M_{xy}\mathrm{d}y - \left(M_{xy} + \frac{\partial M_{xy}}{\partial x}\mathrm{d}x\right)\mathrm{d}y - Q_y\mathrm{d}x\mathrm{d}y = 0, \quad (1b)$$

$$\left(M_x + \frac{\partial M_x}{\partial x}\mathrm{d}x\right)\mathrm{d}y - M_x\mathrm{d}y - M_{yx}\mathrm{d}x + \left(M_{yx} + \frac{\partial M_{yx}}{\partial y}\mathrm{d}y\right)\mathrm{d}x - Q_x\mathrm{d}x\mathrm{d}y = 0, \quad (1c)$$

with $x, y, t \in \mathbb{R}, t \geq 0$, where $q(x, y, t)$ is the differential external load, ρ is the density, and $w(x, y, t)$ measures the deflection of the middle plane of the plate. For point actuated deformable mirrors with N actuators, the external load $q(x, y, t)$ can be written as

$$q(x, y, t) = \sum_{j=1}^{N} \delta(x - x_j)\delta(y - y_j)u_j(t), \quad (2)$$

where $u_j(t)$ is the effective force of one actuator (input) and $\{x_i, y_i\}$ are the actuator locations. Rotary-inertia effects of plate elements as well as higher-order contributions to the moments from loading q have been neglected in the moment equations (1b) and (1c). By canceling terms, the equations of motion reduce to

$$\frac{\partial Q_x}{\partial x} + \frac{\partial Q_y}{\partial y} + q = \rho h\frac{\partial^2 w}{\partial t^2}, \quad (3a)$$

$$\frac{\partial M_y}{\partial y} - \frac{\partial M_{xy}}{\partial x} - Q_y = 0, \quad (3b)$$

$$\frac{\partial M_x}{\partial y} + \frac{\partial M_{yx}}{\partial x} - Q_x = 0. \quad (3c)$$

A single equation in terms of various moments can be achieved by solving the last two equations for Q_x and Q_y and substituting in the first equation yielding

$$\frac{\partial^2 M_x}{\partial x^2} + \frac{\partial^2 M_{xy}}{\partial x \partial y} - \frac{\partial^2 M_{xy}}{\partial y \partial x} + \frac{\partial^2 M_y}{\partial y^2} + q = \rho h\frac{\partial^2 w}{\partial t^2}. \quad (4)$$

In [11] the relationship between the moments and the deflection is further described. It can be shown that the bending moments per unit length read

$$M_x = -D\left(\frac{\partial^2 w}{\partial x^2} + \nu\frac{\partial^2 w}{\partial y^2}\right), \tag{5a}$$

$$M_y = -D\left(\frac{\partial^2 w}{\partial y^2} + \nu\frac{\partial^2 w}{\partial x^2}\right), \tag{5b}$$

$$M_{xy} = -M_{yx} = D(1-\nu)\frac{\partial^2 w}{\partial x \partial y}, \tag{5c}$$

$$D = \frac{Eh^3}{12(1-nu^2)}, \tag{5d}$$

with Young's modulus E and Poisson's ratio ν. By using the relationship $M_{xy} = -M_{yx}$ the biharmonic equation

$$D\left(\frac{\partial^4 w}{\partial x^4} + 2\frac{\partial^4 w}{\partial x^2 \partial y^2} + \frac{\partial^4 w}{\partial y^4}\right) - q = -\rho h\frac{\partial^2 w}{\partial t^2} \tag{6}$$

can be derived. For a circular plate, (6) can be written in polar coordinates as

$$D\nabla^4 w(r,\theta,t) + \rho h\frac{\partial w(r,\theta,t)}{\partial t^2} = q(r,\theta,t), \tag{7}$$

with $r \in [r_1, r_2], \theta \in [0, 2\pi]$, where $\nabla^4 = \nabla^2\nabla^2$, and ∇^2 is the Laplacian in polar coordinates

$$\nabla^4 = \left(\frac{\partial^2}{\partial r^2} + \frac{1}{r}\frac{\partial}{\partial r} + \frac{1}{r^2}\frac{\partial^2}{\partial \theta^2}\right)^2. \tag{8}$$

The boundary conditions for a free edge at the inner and outer radius r_1 and r_2 of the mirror shell (see Fig. 2) read [16]

$$D\left(\frac{\partial^2 w}{\partial r^2} + \frac{\nu}{r}\frac{\partial w}{\partial r} + \frac{\nu}{r^2}\frac{\partial^2 w}{\partial \theta^2}\right)\Big|_{r=\{r_1,\, r_2\}} = 0, \tag{9a}$$

$$D\left[\frac{\partial}{\partial r}\nabla^2 w - (1-\nu)\frac{\partial^2}{\partial \theta^2}\left(\frac{1}{r^2}\frac{\partial w}{\partial r} - \frac{w}{r^3}\right)\right]\Big|_{r=\{r_1,\, r_2\}} = 0. \tag{9b}$$

With (7) and (9), the dynamic behavior of a free homogeneous mirror shell is described. By separation of variables with $w(r,\phi,t) = \sum_{k=1}^{\infty} W(r,\phi)\exp^{(-i\lambda_k t)}$, and $W(r,\phi) = W_{1,k}(r,\phi) + W_{2,k}(r,\phi)$ it is possible to transform (7) into two independent spatial parts

$$(\nabla^2 + \beta_k^2)W_{1,k}(r,\theta) = 0, \quad (\nabla^2 + \beta_k^2)W_{2,k}(r,\theta) = 0, \tag{10}$$

where $\beta_k^4 = \frac{\rho h \lambda_k}{D}$. The solutions of these equations are of the form

$$\begin{aligned} W_{1,k}(r,\theta) &= A_{1,k}J_k(\beta_k r)\sin(k\theta) + A_{2,k}J_k(\beta_k r)\cos(k\theta) + \cdots \\ &\quad \cdots + A_{3,k}Y_k(\beta_k r)\sin(k\theta) + A_{4,k}Y_k(\beta_k r)\cos(k\theta), \end{aligned} \tag{11a}$$

$$\begin{aligned} W_{2,k}(r,\theta) &= B_{1,k}I_k(\beta_k r)\sin(k\theta) + B_{2,k}I_k(\beta_k r)\cos(k\theta) + \cdots \\ &\quad \cdots + B_{3,k}K_k(\beta_k r)\sin(k\theta) + B_{4,k}K_k(\beta_k r)\cos(k\theta), \end{aligned} \tag{11b}$$

where J_k and Y_k are Bessel functions of order k, $k \in \mathbb{N}$ and of the first and second kind, respectively. For the second component W_2, the functions I_k and K_k are modified or hyperbolic Bessel functions of order k and of the first and second kind, respectively. The coefficients $A_{i,k}$ and $B_{i,k}$, $(i = 1 \ldots 4)$, must be determined such that the boundary conditions in (9) are fulfilled. Hence, the solution of (7) is the sum of (11a) and (11b) and has the form

$$\begin{aligned} W_k(r,\theta) = &\left[A_{1,k}J_k(\beta_k r) + A_{3,k}Y_k(\beta_k r) + B_{1,k}I_k(\beta_k r)\right. \\ &\left. + B_{3,k}K_k(\beta_k r)\right]\sin(k\theta) + \ldots \\ &\ldots + \left[A_{2,k}J_k(\beta_k r) + A_{4,k}Y_k(\beta_k r)\right. \\ &\left. + B_{2,k}I_k(\beta_k r) + B_{4,k}K_k(\beta_k r)\right]\cos(k\theta). \end{aligned} \tag{12}$$

In general, the resulting eigenmodes of (12) can be used for a modal approximation of the spatial dynamics of a continuous face-sheet deformable mirror. For the deformable mirror described in [21], additional mechanical influences have to be considered. First of all, the inner radius r_1 is not completely free, but clamped to a central membrane of low rigidity. Also, the deformable mirror contains small magnets that are glued on the backside of the shell as part of the voice coil actuators. Thereby, the assumed homogeneous mass distribution for the derivation of (12) is not fully met. Taking both effects into account, the modes in (12) do not fully describe the spatial dynamics of the shell, yet. However, it can be shown that the central membrane of low rigidity can be included in an analytic formulation

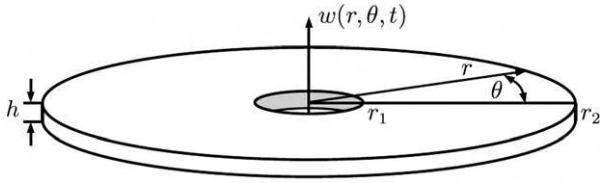

Fig. 2. Principle layout of the deformable mirror modeled as a thin Kirchoff plate.

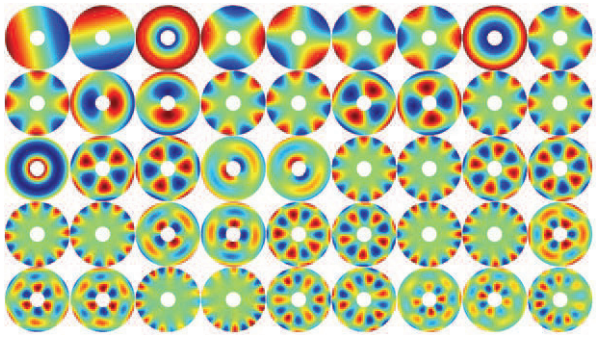

Fig. 3. Finite element analysis results of eigenmodes of the P45 adaptive secondary mirror prototype.

of boundary conditions for the inner radius [23]. Also, the inhomogeneous mass distribution can be compensated for by appropriate local control. In sum, it is possible to derive an orthogonal set of modal basis functions and perform system analysis and control in terms of modal coordinates.

Here, it is assumed that the set of orthogonal eigenmodes is known. For the P45, these modes were justified via finite element analysis and proved validity in vibration tests with the mirror shell.

3. Modal System Identification

Given a set of orthogonal eigenmodes of the mirror, it is essential to derive the temporal behavior of each mode. Especially mode-depend damping must be measured in practice as only little knowledge about viscous damping due to air-gaps between the mirror shell and the reference plate is gained so far. For the P45, the eigenmodes, shown in Fig. 3, were used for modal analysis of the mirror dynamics[1]. The high number of selected modes is chosen to achieve an accurate spatial approximation of the plate dynamics. The modes were derived from finite element simulations with a detailed model of the shell including glued magnets and appropriate boundary conditions [8]. Since the deformable mirror can only be used within active position control, the identification results represent the closed loop system behavior instead of the pure shell dynamics. However, by knowing the controller design of the local position controllers, the shell dynamics can be determined from the closed loop dynamics via closed loop system identification [14, 13]. For the P45, the dynamics of underlying control loops, including voice coil drivers, capacitive sensors and signal conversion, are found to be negligible because they have a cut-off frequency above 4 kHz.

[1] The piston mode was included in the analysis, too. However, the constant term is not shown in Fig. 3.

Similar to assumptions in Section 2, it is presumed that the spatial and temporal behavior of the mirror can be written in an approximate mode-dependent form

$$w(r,\phi,t) = \sum_{i=1}^{M} c_i W_i(r,\phi,t), \tag{13}$$

with mode index i and amplitudes $c_i \in \mathbb{R}$. By using the modal approximation with separation of the spatial and temporal behavior, the eigenmodes $W_i(r,\phi,t)$ can be expanded to

$$W_i(r,\phi,t) = \Omega_i(r,\phi) f_i(t), \tag{14}$$

where $\Omega_i(r,\phi) \in \mathbb{R}^2$ is the ith spatial mode and $f_i(t)$ is the solution of a stable ordinary differential equation in time. Stability is guaranteed, since the measurements were performed in closed loop operation and the local control loops were designed to be stable. Despite the possibility of nonlinear damping, it is assumed that the temporal behavior $f_i(t)$ can be approximated by a linear ODE of order n of the form

$$\begin{aligned} \sum_{j=0}^{n} a_{i,j} \frac{d^j}{dt^j} f_i(t) &= \sum_{j=0}^{m} d_{i,j} \frac{d^j}{dt^j} u_{i,j}(t), \quad t \geq 0,\ f_i(t) \in \mathbb{R}, \\ \frac{d^v}{dt^v} f_i(0) &= \hat{f}_{i,0,v}, \quad v = 0(1)n-1,\ m < n, \end{aligned} \tag{15}$$

where $u_i(t)$ is the modal excitation of the ith mode with coefficients $a_{i,j}$ satisfying the Hurwitz criterion.

For modal identification of the P45, each eigenmode $\Omega_i(r,\phi)$ was excited by a pseudo random binary sequence (prbs) with a frequency range of 30 Hz–30 kHz. The deflection of the excited mirror was recorded at the positions of all 45 actuators with a sampling rate of 60 kHz. The measurement results of all 45 modes are illustrated in Fig. 4. It was found that electronic cross-talk between the actuators and capacitive sensors at frequencies above 4 kHz led to identification problems. Therefore, only the frequency response up to 4 kHz was considered for a subspace based identification of the first 45 eigenmodes in closed loop operation [13, 14, 26]. The frequency truncation is justified by the fact that all 45 modes have their resonant frequencies below 4 kHz as visible in Fig. 3. In the identification process, a second order approximation of the dynamics of the form

$$a_{i,2}\ddot{f}_i(t) + a_{i,1}\dot{f}_i(t) + a_{i,0} f_i(t) = K u_i(t), \quad i = 1(1)45, \tag{16}$$

was found to be sufficient for all 45 modes. By using the measured frequency response of the mirror in closed loop operation, not only the dynamics of the mirror shell, but

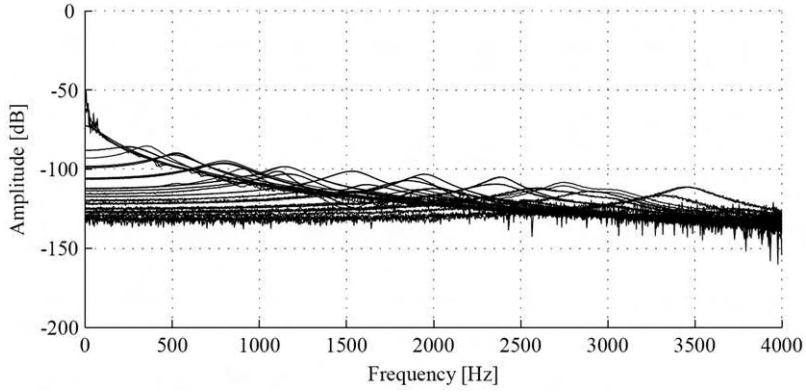

Fig. 4. Frequency response of relevant frequencies for the first 45 eigenmodes measured at the P45.

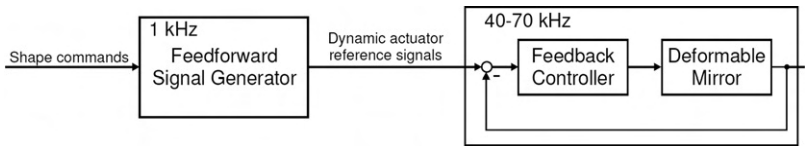

Fig. 5. Control layout of implemented flatness based feedforward control with the P45 deformable mirror.

also actuator and sensor dynamics, and viscous damping are included in the identified modal models.

The identified modal models of the deformable mirror can now be used to design model-based feedforward control signals.

4. Model-Based Feedforward Control

By having suitable modal models for the closed loop behavior of the mirror, it is possible to design dynamic feedforward signals for set-point changes of the shell. The main idea is to drive the mirror shell from one static deformation to another one by accounting for its transient behavior in the input signal rather than by local error feedback. Thereby, the input signals can be designed to achieve desired settling times with limited overshoot of the output signals. For a well-designed trajectory, modeling errors and external disturbances are compensated for by the local error feedback (see Fig. 5).

The feedforward trajectories can be computed at the same frequency as the shape commands for the deformable mirror unit are generated (about 1 kHz). In practice, the trajectories can then be stored in an internal command buffer for each actuator. It is not necessary to compute the local feedforward trajectories at the local control frequency of 40–70 kHz because the set-point change will occur only when a new desired shape is commanded to the mirror unit. In [22], the necessary computation steps are discussed in detail. For practical implementation, e.g. at the Large Binocular Telescope, the computational needs for wavefront reconstruction and trajectory generation must be incorporated carefully to guarantee the feedforward trajectory computation at 1 kHz.

In [22], trajectory generation for a set-point change of a deformable mirror modeled as a linear time invariant second order systems with full relative degree is introduced. Thereby, the main idea is to generate a smooth reference trajectory $y_d(t)$ and compute the desired modal feedforward signal $u_r(t)$ as[2]

$$u_r(t) = \frac{1}{K}\left(a_0 y_d(t) + a_1 \dot{y}_d(t) + a_2 \ddot{y}_d(t)\right). \qquad (17)$$

However, this methodology is only suitable for eigenmodes with low eigenfrequencies and no relevant zero dynamics as observed with the P45. As soon as higher temporal dynamics are needed, additional influences have to be considered. In particular, for future large deformable mirrors it might be necessary to account for higher order disturbances as distributed viscous air-damping and the dynamic influence of the voice coils by additional zeros and poles in the transfer function of each closed loop mode. The resulting modal transfer functions in Laplace domain are then of form

$$Y(s) = \frac{d_0 + d_1 s + \ldots + d_m s^m}{a_0 + a_1 s + \ldots + a_n s^n} U(s), \quad m < n. \qquad (18)$$

In this case, the feedforward signals cannot be computed directly from the reference trajectory $y_d(t)$ as in (17).

[2] The modal index i is ommitted for all variables to improve readability.

Instead, the formalism of differential flatness can be used for feedforward trajectory generation [10, 24]. Thereby, the trajectory generation for model-based feedforward control is formulated for the general class of modal representations of the mirror dynamics by linear systems in state space of the form

$$\begin{aligned}\Sigma: \quad & \dot{\boldsymbol{x}}_i = A_i \boldsymbol{x}_i + \boldsymbol{b}_i u_i, \quad \boldsymbol{x}_i(0) = \boldsymbol{x}_{0i} \in \mathbb{R}^n, \\ & y_i = \boldsymbol{c}_i^T \boldsymbol{x}_i, \quad u_i, y_i \in \mathbb{R}. \end{aligned} \tag{19}$$

where the output y_i is the amplitude of eigenmode i and u_i is the modal input signal, respectively (see (14), (15)).

For differential flatness of (19), the relative degree $0 < r \leq n$ is of importance. For linear systems of form (19) the relative degree is defined as

$$\begin{aligned}0 < r \leq n: \quad & \boldsymbol{c}^T A^{j-1} \boldsymbol{b} = 0, \; j = 1(1)r-1, \\ & \boldsymbol{c}^T A^{r-1} \boldsymbol{b} \neq 0. \end{aligned} \tag{20}$$

By definition, a flat output of (19) has a full relative degree $r = n$. With (20), the determination of a differentially flat output $z = \boldsymbol{\lambda}^T \boldsymbol{x}$ can be performed by

$$\begin{aligned}& \boldsymbol{\lambda}^T \underbrace{[\boldsymbol{b}, A\boldsymbol{b}, \ldots, A^{n-1}\boldsymbol{b}]}_{P} = \underbrace{[0, \ldots, 0, \epsilon \neq 0]}_{\boldsymbol{e}^T} \\ & \Rightarrow \quad \boldsymbol{\lambda}^T = \boldsymbol{e}^T P^{-1} \quad \text{with} \; \operatorname{rank}\{P\} = n. \end{aligned} \tag{21}$$

The flat output $z = \boldsymbol{\lambda}^T \boldsymbol{x}$ is not unique because of the non-zero constant ϵ. Although, in practice $\epsilon = 1$ can be assumed. For trajectory generation, a state transformation into flat coordinates $\boldsymbol{x}^*$ yields

$$\boldsymbol{x}^* = \begin{pmatrix} z \\ \dot{z} \\ \ldots \\ \overset{(n-1)}{z} \end{pmatrix} = \begin{pmatrix} \boldsymbol{\lambda}^T \\ \boldsymbol{\lambda}^T A \\ \ldots \\ \boldsymbol{\lambda}^T A^{n-1} \end{pmatrix} \boldsymbol{x} = T \boldsymbol{x}. \tag{22}$$

With these coordinates, system (19) can be written in the SISO controller normal form

$$\begin{aligned}\Sigma^*: \quad \overset{(n)}{z} = & \underbrace{-[v_0, \ldots, v_{n-1}]}_{-\boldsymbol{v}^T = \boldsymbol{\lambda}^T A^n T^{-1}} \boldsymbol{x}^* + \epsilon u, \\ & \boldsymbol{x}^*(0) = T\boldsymbol{x}_0 \in \mathbb{R}^n, \end{aligned} \tag{23}$$

$$\begin{aligned}y = & \underbrace{[c_1^*, \ldots, c_{n-r+1}^*, 0, \ldots, 0]}_{\boldsymbol{c}^{*T} = \boldsymbol{c}^T T^{-1}} \boldsymbol{x}^* \\ & \text{with} \; c_{n-r+1}^* \neq 0. \end{aligned} \tag{24}$$

With the flat output z, a differential parametrization of the linear SISO system (19) yields

$$\Sigma^{-1}: \quad \boldsymbol{x} = \Psi_x(z) = T^{-1}[z, \dot{z}, \ldots, \overset{(n-1)}{z}]^T, \tag{25}$$

$$u = \Psi_u(z) = (v_0 z + v_1 \dot{z} + \cdots + v_{n-1} \overset{(n-1)}{z} + \overset{(n)}{z})/\epsilon, \tag{26}$$

$$y = \Psi_y(z) = c_1^* z + c_2^* \dot{z} + \cdots + c_{n-r+1}^* \overset{(n-r)}{z}. \tag{27}$$

By these equations, the inverse System Σ^{-1} is described. The flat output trajectory is supposed to be n-times continuously differentiable $z \in \mathcal{C}^n$.

Now, a flatness based feedforward trajectory can be designed for a modal set-point change from $x(0) = \boldsymbol{x}_0$ to $x(t_f) = \boldsymbol{x}_f$. For that purpose, the initial and final states $\boldsymbol{x}_0$ and $\boldsymbol{x}_f$ are transformed into flat coordinates (22). By connecting the flat set-points z_0 and z_f with a n-times continuously differentiable trajectory $z_d(t)$, $t \in [0, t_f]$, the feedforward input $u_d(t)$ can be computed via (26). In literature, various motion primitives exist for continuous set-point changes. For a detailed survey on continuously differentiable trajectories for mechanical application see e.g. [3].

Due to the defined linear structure of the integrator chain (22), a time optimal solution for a $\mathcal{C}^n$ trajectory under output constraints results in switching behavior of the n-th time derivative of $z_d(t)$ [25]. Planning such trajectories usually leads to numerical optimization of the n-th time derivative of $z_d(t)$, including numerical integration and a strong dependency on the chosen time discretization. In order to avoid a discrete description of the trajectory, it is a common technique to describe the trajectory $z_d(t)$ by a polynomial of the form (29). Thereby, the transition time is supposed to be t_f:

$$\begin{aligned}\Sigma_d^*: \quad & z_0 = \boldsymbol{\lambda}^T \boldsymbol{x}_0, \quad z_f = \boldsymbol{\lambda}^T \boldsymbol{x}_f, \\ & \overset{(j)}{z}_d(0) = \overset{(j)}{z}_d(t_f) = 0, \; j = 1(1)n, \end{aligned} \tag{28}$$

$$z_d(t) = z_0 + (z_f - z_0) \sum_{v=n}^{2n-1} p_v \left(\frac{t}{t_f}\right)^v \in \mathcal{C}^n, \tag{29}$$

After inserting the reference trajectory $z_d(t)$ in the input parametrization (26), a continuous feedforward control signal $u_d(t) \in \mathcal{C}^0$ is achieved. Due to the polynomial description of the reference trajectory (29) and the input transformation (26), the resulting feedforward trajectory is a polynomial of order $2n-1$. The polynomial coefficients can easily be computed for all eigenmodes and used for on-line feedforward signal generation. By adjusting the traveling time t_f, the evolution of $u_d(t)$ can be

influenced and dynamic constraints on the input signal can be accounted for [22]. The reference signal $y_d(t)$ is derived from (27). In Fig. 6, the proposed feedforward and feedback control scheme for future deformable secondary mirrors is shown. It must be noted that the reference trajectories $y_d(t)$ and $u_d(t)$ can be computed off-line for arbitrary set-point changes in advance. For practical use, they can be stored in internal memory of the deformable mirror's control system allowing fast feedforward signal generation.

5. Experimental Results and Chopping Simulations

The identification results of eigenmodes at the P45 allowed to derive a model of the mirror dynamics for the first 45 eigenmodes. For the piston mode, the feedforward trajectory generation concept described in Section 4 was applied practically. The control task was to drive the mirror from relative position 0 µm to 1 µm in piston. It must be noted that the local control loops were used with proportional position feedback only and no electronic damping both for the identification and feedforward control measurements

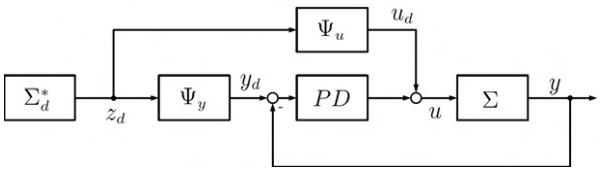

Fig. 6. Proposed modal two-degree-of-freedom control scheme with *PD*–output control for modal dynamics of system Σ, trajectory generation Σ_d^*, feedforward control Ψ_u and input filter Ψ_y.

was used. The piston mode was chosen because it has no intrinsic damping. Together with the tip and tilt modes it does not cause the plate to bend and therefore represents the worst case scenario of mirror dynamics. For the computation of the needed input signals $\hat{u}_v$ for all actuators $v = 1(1)45$, a modal reference trajectory of form (29) with transition time of $t_f = 1$ ms was chosen for the flat modal output of the piston mode. For the small scale deformable mirror P45, higher order dynamics were found to be insignificant and no zero dynamics were included in the identified modal model. Therefore, the flat modal output is equivalent to the physical modal output. With (26), the modal feedforward signal for the piston mode was computed. The derived modal feedforward signal u_d of the piston mode was then transformed into actuator coordinates $\hat{u}_v$ and used as feedforward signals for all underlying control loops, respectively. Thereby, the transformation accounted for varying actuator efficiencies that were identified earlier. The spatial evolution of the step response with and without model-based feedforward control is shown in Figures 7 and 8 for selected time instances. The mirror surface was reconstructed with the 45 position measurements at each actuator and additional 2D cubic spline interpolation between the actuators.

For the static step response, it must be mentioned that not only the piston mode was excited during the experiments, but also some higher spatial frequency modes. In order to gain an impression of only the dynamics of the piston mode, the experimental results are illustrated in a modal transformation in Fig. 9. The settling time with pure static feedforward commands and no electronic damping was found to be 2.7 ms. In contrast, with model-based feedforward control the specified settling time of 1 ms was met and only little overshoot within the tolerance of 10%

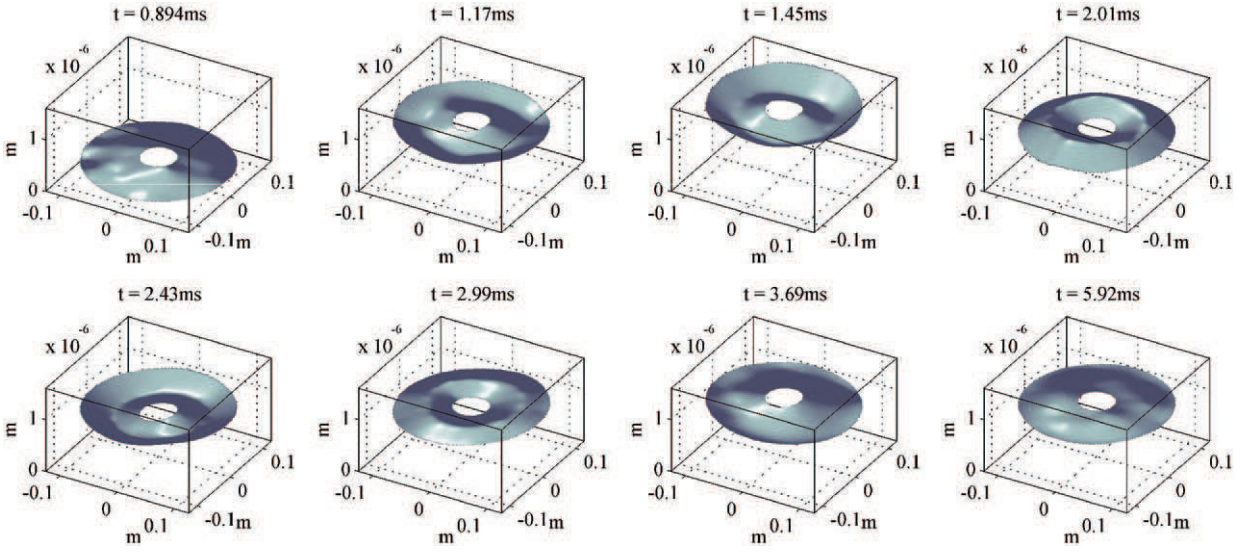

Fig. 7. Measurement results of the step response of 1 µm for the piston mode of the P45 with proportional feedback control.

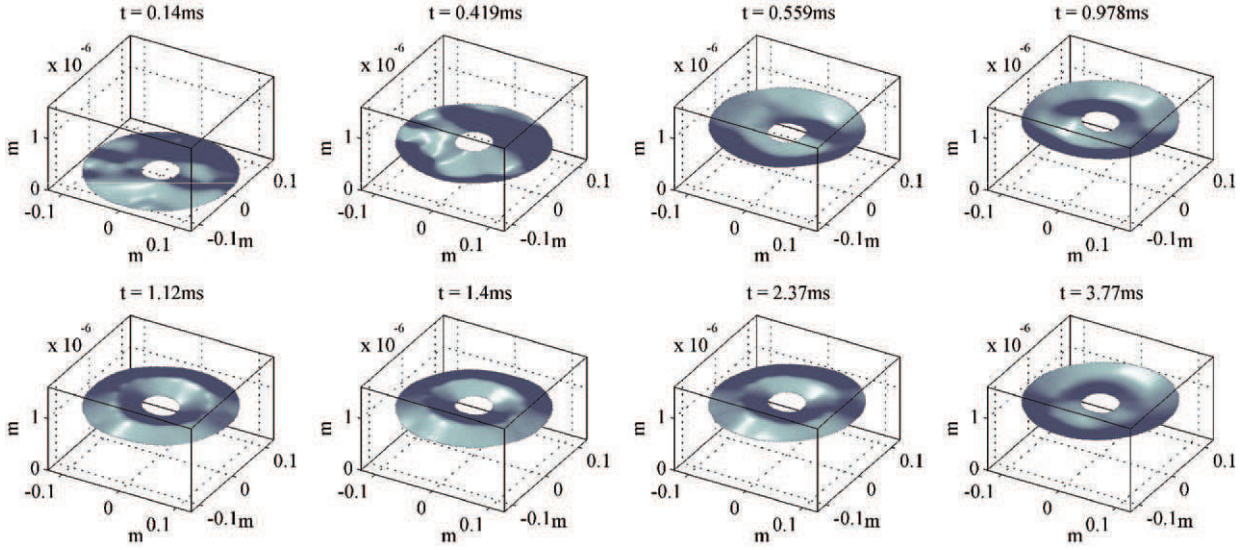

Fig. 8. Measurement results of the step response of 1 µm for the piston mode of the P45 with pure proportional feedback control and flatness based feedforward control.

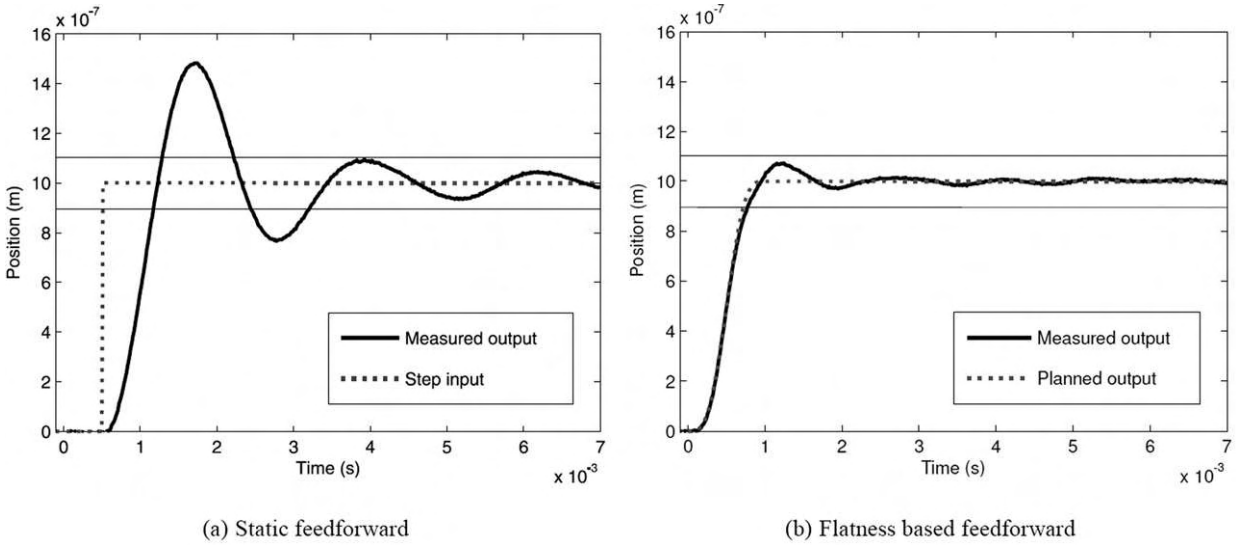

Fig. 9. Modal projection of measurement results of a set-point change of 1 µm in piston with and without flatness based feedforward control.

nominal can be seen. Also, the measurements show only little spillover to higher spatial frequency modes which is a result of efficiency based signal generation for all actuators.

Comparable results for set-point changes of the P45 with local PD-control and without flatness based feedforward control are presented in [19]. In contrast, the main advantage of additionally using flatness based feedforward control is that the local position controllers can be tuned to achieve closed loop stability and robustness explicitly. In practice, it turns out to be a very delicate task to tune the parameters of the local controllers such that both tracking performance and robustness are achieved in combination for various deformations of the mirror shell. Also, neighboring position control loops must be designed not to have a negative influence on each other in terms of global stability. By using model-based feedforward control for large set-point changes, the tracking performance can be addressed separately and negative effects of interacting actuators can be reduced significantly leading to simplified feedback controller design.

In order to show the usability of model-based feedforward control for demanding mirror commands, mirror chopping is analyzed further now. Chopping is a technique

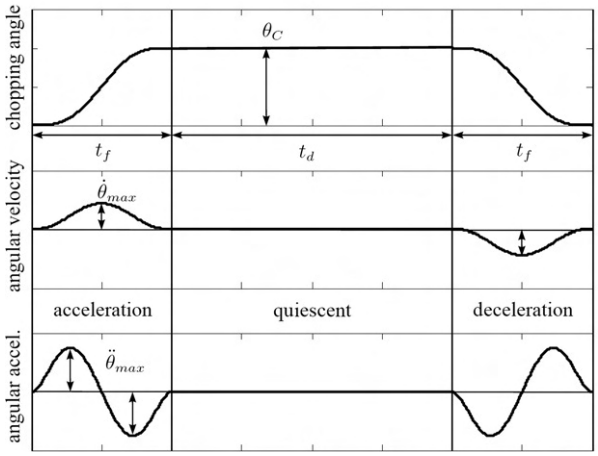

Fig. 10. Modal chopping trajectory $\theta_d(t)$ with peak-to-peak amplitude θ_C, transition time t_f, and duty cycle time t_d based on $\mathcal{C}^7$ transition polynomials.

of spatially switching the telescope line of sight in order to improve the signal-to-noise ratio for weak sources on sky. Spatial chopping essentially requires that one of the elements of the optical path is precisely positioned in each of two angular orientations in order to direct the telescope line of sight to either the source under observation or an area of blank sky containing only background noise. Although, in theory, any element of the optical path can be used to chop the incoming beam, the secondary mirror has been chosen as the best optical element with which to implement chopping in the cassegrain optical designs used for most large telescopes [15]. For the P45, the modal frequency response of the chopping mode was measured. Thereby, the temporal behavior of the chopping mode can be reconstructed and a simulation of the resulting chopping command with appropriate feedforward signals can be performed.

The desired chopping behavior is defined by three parameters: the amplitude of the chop command (peak-to-peak) θ_C, the transition time t_f, and the duty cycle time t_d. A typical waveform time profile shown in Fig. 10 consists of acceleration, deceleration, and quiescent phases. The transition time t_f is effecting the angular velocity $\dot{\theta}$ and acceleration $\ddot{\theta}$ of the mirror and is limited due to maximum force capabilities of included voice coil actuators. For a transition polynomial of order 7, the transition time t_f can be computed as

$$t_f = \max\left\{\frac{\theta_C}{2\dot{\theta}_{\max}}, \sqrt{\frac{3003}{1024}\frac{\theta_C}{\ddot{\theta}_{\max}}}\right\}. \tag{30}$$

For the LBT adaptive secondary, chopping up to $\pm 5''$ shall be achieved in not more than 20 ms. Given the transition profile (29), a flatness based feedforward trajectory

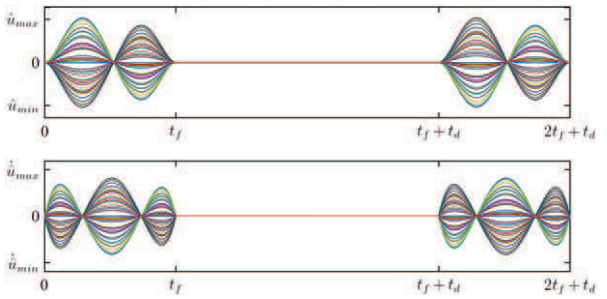

Fig. 11. Simulated chopping input commands for all actuators of the P45 in normalized units.

for the chopping mode can be computed in the following way:

$$z_{1,1}(t) = z_0 + (z_C - z_0)\left(35\left(\frac{t}{t_f}\right)^4 - 84\left(\frac{t}{t_f}\right)^5 + 70\left(\frac{t}{t_f}\right)^6 - 20\left(\frac{t}{t_f}\right)^7\right), \quad 0 \le t \le t_f \tag{31}$$

$$z_{1,2}(t) = z_C, \quad t_f \le t \le t_f + t_d, \tag{32}$$

$$z_{1,3}(t) = z_C + (z_0 - z_C)\left(35\left(\frac{t-t_1}{t_f}\right)^4 - 84\left(\frac{t-t_1}{t_f}\right)^5 + 70\left(\frac{t-t_1}{t_f}\right)^6 - 20\left(\frac{t-t_1}{t_f}\right)^7\right), \quad t_f + t_d \le t \le 2t_f + t_d,\ t_1 = t_f + t_d. \tag{33}$$

Hereby, the initial and final conditions are derived via a modal state transformation (14) and (22). The modal feedforward commands $u_{1,1}(t)$, $u_{1,2}(t)$, $u_{1,3}(t)$ can then be computed via (26). A transformation from modal to physical coordinates $\hat{u}$ finally leads to the desired input trajectories exemplary shown in normalized units for the P45 in Fig. 11.

The sign-switching feedforward trajectories for all 45 actuators can be saved off-line and used for chopping as needed.

6. Conclusions

In this paper, a model-based feedforward control concept for faster settling times and less overshoot for set-point changes of large deformable mirrors was proposed. Thereby, the possibility to take local position control loops of excited actuators and mode-dependent stiffness variations of the mirror shell into account was demonstrated. Based on validated dynamical model of the mirror shell, a modal approximation of the mirror dynamics was performed. For describing the dynamics of the eigenmodes, appropriate transfer functions were found by

modal analysis with a 45-actuator prototype of the Large Binocular Telescope adaptive secondary mirror (P45). Additionally, the challenging task of mirror chopping was addressed and simulation results with model-based feedforward trajectories were shown for chopping.

In conclusion, feedforward control proofed to be a valuable add-on for existing and future deformable mirrors. Especially for large amplitude set-point changes, the concept of model-based feedforward control can greatly simplify local position control design and support overall system performance. The additional computational load for feedforward signal generation is expected to be comparably low because it can be performed in the higher level wavefront control loop cycle running at a lower frequency (about 1 kHz) than the local position control loops (40–70 kHz).

In the future, concepts for closed-loop system identification of large deformable mirrors have to be developed. Especially the influences of viscous damping need to be investigated further. With the finishing of the two deformable secondary mirrors for the LBT, further measurement runs and practical verification of model-based chopping are aspired.

Acknowledgment

The authors would like to acknowledge the major support of the Asstrofisico di Arcetri by providing the finite element data of the P45, the measurement time with the large deformable mirror prototype, and data concerning the layout and control schemes of the LBT deformable secondary mirrors. Additionally, the authors would like to thank M. Zeitz for fruitful discussions and technical advise in the theory of flat systems. Furthermore, the authors would like to thank the reviewers for their valuable comments.

This work was supported by the DFG under grant SA-847/10-1 and OS-111/29-1.

References

1. Arsenault R, Biasi R, Gallieni D, Riccardi A, Lazzarini P, Hubin N, Fedrigo E, Donaldson R, Oberti S, Stroebele S, Conzelmann R, Duchateau M. A deformable secondary mirror for the VLT. *Society of Photo-Optical Instrumentation Engineers (SPIE) Conference Series*, *Society of Photo-Optical Instrumentation Engineers (SPIE) Conference Series* 2006; 6272. doi:10.1117/12.672879.
2. Baudouin L, Prieur C, Guignard F, Arzelier D. Robust control of a bimorph mirror for adaptive optics systems. *Appl Opt* 2008; 47(20): 3637–3645.
3. Biagiotti L, Melchiorri C. *Trajectory Planning for Automatic Machines and Robots.* Springer, 2008.
4. Biasi R, Andrighettoni M, Veronese D, Biliotti V, Fini L, Riccardi A, Mantegazza P, Gallieni D. LBT adaptive secondary electronics. *Society of Photo-Optical Instrumentation Engineers (SPIE) Conference Series* 2003; 4839: 772–782. doi: 10.1117/12.458951.
5. Bruns DG, Sandler DG, Martin B, Brusa G. Design and prototype tests of an adaptive secondary mirror for the new 6.5-m single-mirrorMMT. *Society of Photo-Optical Instrumentation Engineers (SPIE) Conference Series* 1995; 2534: 130–133.
6. Brusa G, Riccardi A, Ragland S, Esposito S, del Vecchio C, Fini L, Stefanini P, Biliotti V, Ranfagni P, Salinari P, Gallieni D, Biasi R, Mantegazza P, Sciocco G, Noviello G, Invernizzi S. Adaptive secondary P30 prototype: laboratory results. Bonaccini D, Tyson RK (eds.). *Adaptive Optical System Technologies*, *Society of Photo-Optical Instrumentation Engineers (SPIE) Conference Series*, 1998; 3353: 764–775.
7. Brusa G, Riccardi A, Salinari P, Wildi FP, Lloyd-Hart M, Martin HM, Allen R, Fisher D, Miller DL, Biasi R, Gallieni D, Zocchi F. MMT adaptive secondary: performance evaluation and field testing. Peter LW (ed.). *Adaptive Optical System Technologies II. Bonaccini, Domenico*, *Society of Photo-Optical Instrumentation Engineers (SPIE) Conference Series* 2003; 4839: 691–702.
8. Del Vecchio C, Gallieni D. Numerical simulations of the LBT adaptive secondary mirror. *Society of Photo-Optical Instrumentation Engineers (SPIE) Conference Series* 2000; 4007: 516–523.
9. Fliess M, L'evine J, Martin P, Rouchon P. Flatness and defect of non-linear systems: introductory theory and examples. *Int J Control* 1995; 61(6): 1327–1361.
10. Fliess M, Levine J, Rouchon P. A simplified approach of crane control via a generalized state-space model. *Proceeding of 30th IEEE Conference on Decision and Control* 1991; 1: 736–741. doi:10.1109/CDC.1991.261409.
11. Graff KF. *Wave Motion in Elastic Solids.* Dover Publications, 1991.
12. Hamelinck R, Rosielle N, Kappelhof P, Snijders B, Steinbuch M. A large adaptive deformable membrane mirror with highactuator density. *Society of Photo-Optical Instrumentation Engineers (SPIE) Conference Series* 2004; 5490: 1482–1492. doi:10.1117/12.551070.
13. Katayama T. *Subspace Methods for System Identification.* Springer, 2005.
14. Ljung L, Ljung EJ. *System Identification: Theory for the User*. Prentice-Hall Englewood Cliffs, New Jersey, 1987.
15. Lorell KR, Aubrun J-N, Feher GJ, Perez EO, Zacharie DF, Reshatoff PJ Jr. A high performance chopping secondary mirror for infrared astronomy. Melugin RK (ed.). *Society of Photo-Optical Instrumentation Engineers (SPIE) Conference Series*, *Presented at the Society of Photo-Optical Instrumentation Engineers (SPIE) Conference*, 1993; 1765: 172–184.
16. Meirovitch L. *Analytical Methods in Vibration.* The Mcmillan Company, New York, 1967.
17. Miller DW, Grocott SC. Robust control of the Multiple Mirror Telescope adaptive secondary mirror. *Opt Eng* 1999; 38: 1276–1287. doi:10.1117/1.602186.
18. Riccardi A, Brusa G, Salinari P, Busoni S, Lardiere O, Ranfagni P, Gallieni D, Biasi R, Andrighettoni M, Miller S, Mantegazza P. Adaptive secondary mirrors for the Large binocular telescope. Tyson RK, Lloyd-Hart M (eds.). *Astronomical Adaptive Optics Systems and Applications. ;resented at the Society of Photo-Optical Instrumentation Engineers (SPIE) Conference* 2003a; 5169: 159–168.
19. Riccardi A, Brusa G, Salinari P, Busoni S, Lardiere O, Ranfagni P, Gallieni D, Biasi R, Andrighettoni M, Miller S, Mantegazza P. Adaptive secondary mirrors for the Large

binocular telescope. Tyson RK, Lloyd-Hart M (eds.). *Society of Photo-Optical Instrumentation Engineers (SPIE) Conference Series. Presented at the Society of Photo-Optical Instrumentation Engineers (SPIE) Conference* 2003b; 5169: 159–168. doi:10.1117/12.511374.

20. Riccardi A, Brusa G, Salinari P, Gallieni D, Biasi R, Andrighettoni M, Martin HM. Adaptive secondary mirrors for the large binocular telescope. *Adap Opt Syst Technol II* 2003; 4839(1): 721–732. doi:10.1117/12.458961.
21. Riccardi A, Xompero M, Zanotti D, Busoni L, Del Vecchio C, Salinari P, Ranfagni P, Brusa Zappellini G, Biasi R, Andrighettoni M, Gallieni D, Anaclerio E, Martin HM, Miller SM. The adaptive secondary mirror for the Large Binocular Telescope: results of acceptance laboratory test. *Society of Photo-Optical Instrumentation Engineers (SPIE) Conference Series*, *Society of Photo-Optical Instrumentation Engineers (SPIE) Conference Series* 2008; 7015: doi:10.1117/12.790527.
22. Ruppel T, Lloyd-Hart M, Zanotti D, Sawodny O. Modal trajectory generation for adaptive secondary mirrors in astronomical adaptive optics. *Proceeding of IEEE International Conference on Automation Science and Engineering CASE 2007* 2007; 430–435. doi:10.1109/COASE.2007.4341799.
23. Ruppel T, Osten W, Sawodny O. Adaptive optics simulation with mechanically motivated basis functions. Ellerbroek BL, Hart M, Hubin N, Wizinowich PL (eds.). *Proc SPIE* 2010; 7736: 77363Y. doi:10.1117/12.856023.
24. Sira-Ramirez H, Agrawal SK. *Differentially Flat Systems*. CRC, 2004.
25. Sonneborn LM, Van Vleck FS. *The Bang-Bang Principle for Linear Control Systems*. SIAM, 1964.
26. Van Overschee P. *Subspace Identification for Linear Systems: Theory, Implementation*. Kluwer Academic Publishers, 1996.
27. Vlasov VZ. *Allgemeine Schalentheorie und ihre Anwendung in der Technik*. Akademie-Verlag, 1958.
28. Vogel CR, Yang Q. Modeling and open-loop control of point-actuatied, continuous facesheet deformable mirrors. *Society of Photo-Optical Instrumentation Engineers (SPIE) Conference Series*, *Society of Photo-Optical Instrumentation Engineers (SPIE) Conference Series* 2006; 6272. doi:10.1117/12.669867.